Agricultural and Forest Meteorology 276–277 (2019) 107627

Contents lists available at ScienceDirect

Agricultural and Forest Meteorology

journal homepage: www.elsevier.com/locate/agrformet

# Three dimensional mapping of forest canopy equivalent water thickness using dual-wavelength terrestrial laser scanning

Ahmed Elsherif[a,*], Rachel Gaulton[a], Alexander Shenkin[b], Yadvinder Malhi[b], Jon Mills[a]

[a] School of Engineering, Newcastle University, Newcastle, NE1 7RU, United Kingdom
[b] Environmental Change Institute, University of Oxford, South Parks Road, Oxford OX1 3QY, United Kingdom

ARTICLE INFO

*Keywords:*
Forest health
Forest wildfire
Water stress
Leaf water content
Ground-Based LiDAR.

ABSTRACT

Globally, forests are being subjected to numerous threats, including climate change, wildfires, and insect and disease outbreaks, among others. Satellite optical remote sensing data have been widely utilized in early detection of tree and forest stress by estimating water status metrics such as the leaf Equivalent Water Thickness (EWT). This estimate, however, is affected by soil characteristics and understory vegetation and often ignores the effects of the fine-scale heterogeneity of canopy structure and leaf water content. Such effects can be better understood by studying the EWT distribution in three dimensions. In this study, Terrestrial Laser Scanning (TLS) intensity data from the commercially-available Leica P20 and P40 instruments (808 nm and 1550 nm respectively) were combined in a Normalized Difference Index (NDI). NDI was used to map EWT of 12 trees in three dimensions from floor to canopy in a mixed broadleaf forest plot (Wytham Woods, UK). The average error in EWT estimates across three species was less than 8%. The three dimensional point clouds revealed that, in this snapshot, EWT changes vertically, usually increasing towards canopy top. The proposed method has the potential to provide predawn EWT measurements, is independent of solar illumination, and can lead to a better understanding of the factors affecting satellite estimation of EWT.

## 1. Introduction

Forests are of great importance for humankind and the environment because of the essential ecological, economic and social services they provide (Yao et al., 2014). They play a major role in the global carbon and hydrological cycles (Pan et al., 2011), and influence the climate as a result of exchanging water, energy, carbon dioxide, and other chemicals with the atmosphere (Bonan, 2008). However, natural and anthropogenic threats, such as climate change, drought, disease infections, pest infestations, wildfires, land use change and deforestation, threaten forest health (Lewis et al., 2015; Millar and Stephenson, 2015). Forest health monitoring is critical to understand how forests react to such stressors (Ferretti, 1997; Trumbore et al., 2015), and also for early detection of drought stress, symptoms of disease, and risk of wildfire (Meentemeyer et al., 2008).

Optical remote sensing data, airborne and spaceborne, have been widely adopted in forest health monitoring to overcome the limitations of *in situ* approaches (destructive methods and field spectroscopy), which are time and effort consuming and impractical for large areas (Dash et al., 2017; Pu et al., 2003). Methods that utilize multispectral and hyperspectral optical remote sensing data can provide estimates of vegetation water status metrics, such as the leaf Equivalent Water Thickness (EWT) (g $cm^{-2}$), at landscape level (Clevers et al., 2010; Colombo et al., 2008). EWT can reflect the physiological status of vegetation, as water in vegetation is involved in all physiological processes, directly or indirectly, and lack of water affects plant transpiration rate, photosynthesis rate, and carbon gain (Carter, 1993; Lisar et al., 2012; Peñuelas et al., 1994). EWT can also be linked to other key vegetation water status metrics, including Canopy Water Content (CWC) (kg $m^{-2}$), a parameter of interest in studying water cycle and its role in the global climate change (Clevers et al., 2010), Fuel Moisture Content (FMC), an important metric in prediction and modelling of forest wildfire (Danson and Bowyer, 2004), and Vegetation Water Content (VWC) (kg $m^{-2}$), a key metric in retrieving soil moisture content under vegetation canopies from active and passive microwave remote sensing (Yilmaz et al., 2008).

EWT, defined as the amount of liquid water in a given leaf area (Danson et al., 1992), is estimated from optical remote sensing data using vegetation indices or inversion of radiative transfer models (*e.g.* Serrano et al. (2000); Zhao et al. (2016); Pasqualotto et al. (2018)). However, EWT can only be estimated during the day, as the sensors are dependent on the solar illumination, while determining the vegetation

* Corresponding author.
*E-mail address:* a.m.a.elsherif2@newcastle.ac.uk (A. Elsherif).

https://doi.org/10.1016/j.agrformet.2019.107627
Received 5 February 2019; Received in revised form 16 May 2019; Accepted 17 June 2019
Available online 20 June 2019

water status predawn is preferable as there is no transpiration (Améglio et al., 1999). In addition, the EWT estimation from optical remote sensing data is affected by the canopy structure, understory vegetation, background soil, atmosphere, and shadows, as these factors affect the canopy reflectance and the signal received by the sensor (Ali et al., 2016; Baret and Guyot, 1991; Zarco-Tejada et al., 2003). Furthermore, the vertical heterogeneity in the canopy biophysical and biochemical traits affects the light penetration and scattering within canopy, and thus plays a role in the canopy reflectance; a role that still needs to be further investigated (Ciganda et al., 2008; Liu et al., 2015; Valentinuz and Tollenaar, 2004; Wang and Li, 2013). Thus, in recent years, there have been attempts to utilize Terrestrial Laser Scanning (TLS) data to provide 3D estimates of vegetation EWT to address the aforementioned limitations, in addition to being an active sensor that can provide EWT estimates both midday and predawn.

TLS instruments typically record 3D coordinates and intensity data for each point in the scan, in a high definition point-cloud. The point cloud geometry can be used to obtain numerous forest biophysical attributes (Zheng et al., 2016), while the intensity data can be linked to the canopy reflectance after calibration (Penasa et al., 2014). Calibration is needed for numerous factors that affect the TLS intensity data, including the instrumental effects, the effects of the target distance, and the effects of the incidence angle of the laser beam. Such effects have been highlighted in numerous studies, and methods to calibrate the intensity to apparent reflectance have been successfully developed for various TLS instruments (Anttila et al., 2016; Blaskow and Schneider, 2014; Elsherif et al., 2018; Höfle and Pfeifer, 2007; Jutzi and Gross, 2009; Kaasalainen et al., 2011; Krooks et al., 2013; Tan and Cheng, 2016; Zhu et al., 2017). The calibrated TLS intensity data can then be used to estimate EWT in 3D, using a single shortwave infrared laser wavelength (Zhu et al., 2015; Zhu et al., 2017) or a Normalized Difference Index (NDI) of two laser wavelengths (Elsherif et al., 2018; Gaulton et al., 2013; Junttila et al., 2018, 2016). Using NDI is preferable, as it does not require correction for the incidence angle effects (Elsherif et al., 2018; Hancock et al., 2017), or for the leaf internal structure effects (Ceccato et al., 2001), if the two wavelengths involved in NDI are similarly affected. The leaf internal structure significantly affects the interaction of radiation with foliage (Jacquemoud and Baret, 1990), and calibrating for such effects using a single wavelength is not trivial.

A few recent successful attempts to estimate EWT using TLS data can be found in the literature. Gaulton et al. (2013) found a strong relationship ($R^2$ = 0.80) between EWT of leaf samples from different species and the NDI of near infrared (1064 nm) and shortwave infrared (1545 nm) wavelengths. Zhu et al. (2015) reported a significant correlation ($R^2$ = 0.76) between EWT of leaf samples from eight species and the intensity data from a RIEGL VZ-400 scanner (1550 nm shortwave infrared). Zhu et al. (2017) used data from the same instrument to retrieve the EWT vertical profiles for 20 plants from four different species, observing some vertical heterogeneity in the canopy EWT. Junttila et al. (2016) reported a strong relationship ($R^2$ = 0.93) between EWT of leaf and needle samples from five different species and the NDI of red (690 nm) and shortwave infrared (1550 nm) wavelengths. The relationship between EWT of Norway spruce seedlings and the NDI of 905 nm and 1550 nm wavelengths was investigated by Junttila et al. (2018), with a strong relationship ($R^2$ = 0.91) being reported. Elsherif et al. (2018) showed that the NDI of 808 nm and 1550 nm wavelengths, employed in the Leica P20 and the Leica P40 TLS instruments respectively, was highly correlated to EWT at leaf level ($R^2$ of 0.91 and 0.74) and at canopy level ($R^2$ of 0.89 and 0.74) for deciduous (*Acer davdii*) and conifer (*Pinus nigra*) species respectively, also reporting some heterogeneity in the EWT vertical profiles. However, all the aforementioned studies investigated the relationship between TLS data and EWT at leaf level only, or at leaf and canopy level for small individual trees in a controlled environment. To our knowledge, no successful attempts to utilize TLS data to map the EWT in 3D in real forest environments have been reported in the literature to date.

**Table 1**
Leica P40 and P20 technical specifications.

| | Leica P40 | Leica P20 |
|---|---|---|
| Measurement type | Time-of-flight | Time-of-flight |
| Wavelength | 1550 nm | 808 nm |
| Beam divergence | 0.23 mrad | 0.20 mrad |
| Beam diameter at exit | 3.5 mm | 2.8 mm |
| Beam diameter at 10 m | 5.8 mm | 4.8 mm |
| Beam diameter at 20 m | 8.1 mm | 6.8 mm |
| Maximum range | up to 180 m at 18% reflectivity | up to 120 m at 18% reflectivity |
| Scan rate | up to 1,000,000 points/second | up to 1,000,000 points/second |

In this study, the NDI of the 808 nm near infrared and 1550 nm shortwave infrared wavelengths, employed in the Leica P20 and P40 TLS instruments respectively, was used to produce 3D estimations of EWT in a forest plot in Wytham Woods, Oxford, UK. The aims of the study were to: (i) investigate the effects of leaf internal structure on NDI of the aforementioned wavelengths, (ii) test the ability of NDI to generate 3D EWT estimates in a mixed-species forest plot, and (iii) examine the vertical variation of EWT within forest canopies.

## 2. Materials and methods

### 2.1. TLS instruments

The technical specifications of the Leica P40 and P20 TLS instruments are given in Table 1. Methods to calibrate the intensity data to apparent reflectance for the two instruments are described in Elsherif et al. (2018). A different P40 instrument was used in this study, and access to the P40 and P20 raw intensity data, before the instruments internally apply intensity stretching to enhance the visual appearance of the point clouds, was granted by the manufacturer, Leica Geosystems. Thus, the intensity calibration models were updated. Details are given in Appendix A.

### 2.2. Leaf internal structure effects on NDI

The leaf internal structure not only affects how light interacts with foliage, it also varies between different species and within each individual species (Lichtenthaler et al., 1981). Thus, the ability of NDI of the 808 nm and 1550 nm wavelengths to minimize such effects is a key parameter in estimating EWT at canopy level in forest environments. PROSPECT simulations were conducted to investigate such ability.

PROSPECT (Jacquemoud and Baret, 1990) is a radiative transfer model capable of simulating the optical properties of plant leaves over the visible, near infrared and shortwave infrared regions of the electromagnetic spectrum. The version used in this study was PROSPECT-5 (Feret et al., 2008), which models the leaf optical properties using six parameters: leaf structure coefficient (N), chlorophyll a and b content ($C_{ab}$), carotenoid content ($C_{ar}$), brown pigment content ($C_b$), leaf water content ($C_w$) and dry matter content ($C_m$). The values of $C_{ab}$, $C_{ar}$ and $C_b$ were kept constant at model defaults in all simulations, 47.7 μg $cm^{-2}$, 4.4 μg $cm^{-2}$ and 0 respectively, as they have minor effects on the near and shortwave infrared wavelengths (Gaulton et al., 2013). N is the leaf mesophyll structure coefficient and is related to the cellular arrangement within the leaf (Jacquemoud and Baret, 1990). $C_m$ represents the leaf dry matter content and is quantified in the model as the Leaf Mass per Area (LMA) (Feret et al., 2008), which is the leaf dry weight divided by the leaf surface area (Poorter et al., 2009). $C_m$ will be referred to as LMA and $C_w$ will be referred to as EWT in the remainder of this study. The simulations investigated the effects of N and LMA on NDI and on the NDI – EWT relationship.

**Table 2**
Values of N and LMA used in PROSPECT simulations.

| | Minimum | Interval | Maximum | Reference |
|---|---|---|---|---|
| N | 1.5 | 0.1 | 2.5 | (Jacquemoud and Baret, 1990) |
| LMA (g $cm^{-2}$) | 0.0017 | 0.001 | 0.0157 | LOPEX dataset (Feret et al., 2008) |

#### 2.2.1. The effects of N and LMA on the NDI

EWT was constant at an average value of 0.01 g $cm^{-2}$ in all simulations. LMA was constant at 0.01 g $cm^{-2}$ while N was incrementally changed as shown in Table 2. Next, N was constant at 2 (dimensionless) and LMA was changed following Table 2. NDI was calculated for each simulation.

#### 2.2.2. The effects of N and LMA on the NDI – EWT relationship

A total number of 111 EWT values, ranging between 0.0046 and 0.0162 g $cm^{-2}$, which resulted from actual leaf sample EWT measurements conducted in this study (Section 2.4.1) and in Elsherif et al. (2018), were used. For each EWT value, the simulations described in Section 2.2.1 were conducted. The total number of simulations conducted was 1221 to study the effects of N, and 1665 to study the effects of LMA. The NDI was calculated for each simulation.

### 2.3. Study area and TLS scanning setup

The data collection campaign took place in Wytham Woods near Wytham village (51.78 °N, 1.31 °W) in Oxfordshire, UK, between 22nd and 31st of May 2017. Wytham Woods, owned by the University of Oxford, is one of the most important sites for ecological research in the world (Morecroft et al., 2001). The fieldwork data were acquired in a 35 × 45 m rectangular plot around the treetop canopy walkway in the 18 ha Wytham core plot (Figs. 1 and 2). Wytham core plot is a permanent sample plot, established in the woodland for research purposes (McMahon et al., 2015). The site was dominated by *Quercus robur* (oak) and *Acer pseudoplatanus* (sycamore) trees, in addition to a number of *Fagus sylvatica* (beech) and *Fraxinus excelsior* (ash) trees. The fieldwork campaign took place in non-windy, non-rainy conditions at an average temperature of 21 °Celsius. Thirteen trees around the canopy walkway were selected for sampling, based on how accessible their leaves were from the canopy walkway (Fig. 2). Ten scanning positions were set around the walkway in locations corresponding to low density canopy cover to obtain as much detail (laser beam returns) as possible from the thirteen sampled trees (Fig. 2). At each scan position, full-hemisphere scans (360° × 270°) were conducted by the P40 and the P20 instruments, mounted consecutively on the same tripod, with a resolution (point spacing) of 3 mm at 10 m. Four Leica black and white registration targets were used to link each pair of consecutive scanning positions. The scans were conducted over a period of two days. On the first day, TLS data was collected from scanning positions S1 to S6, with the duration of each scan being approximately fifteen minutes for each instrument. This was followed by leaf sampling, for the purpose of validating the EWT estimation (Section 2.4.2), from trees number 1, 2, 3, 4, 5, 6, and 8. No samples for validation were collected from the ash tree, labelled 7, as it was the only ash tree accessible from the treetop canopy walkway, and samples for building the EWT estimation model were collected from it (Section 2.4.1). On the second day, scans were carried out from scanning positions S7 to S10, followed by collecting leaf samples for validation from trees number 9, 10, 11, 12, and 13. Afterwards, leaf samples for building the EWT estimation models were collected and processed as described in Section 2.4.1.

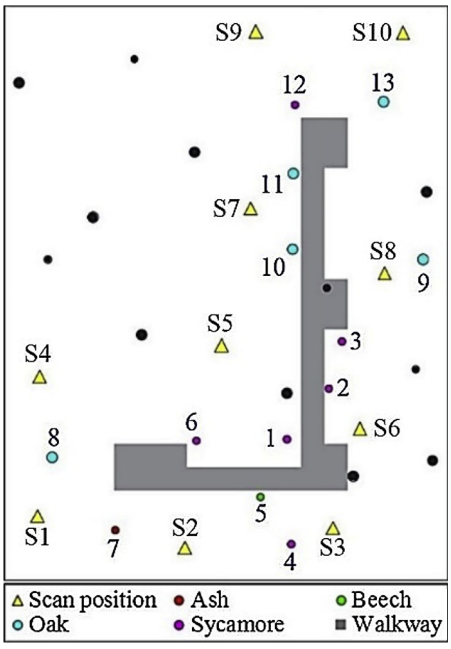


**Fig. 2.** The 35 × 45 m rectangular plot and the thirteen sampled trees (indicated by numbers assigned during fieldwork). Black indicates trees that were not sampled.

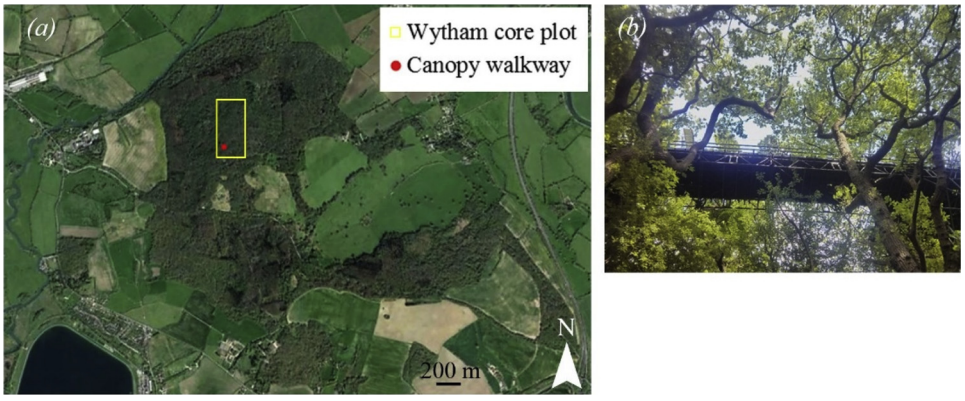


**Fig. 1.** The study area: *(a)* Wytham woods and the location of Wytham core plot and *(b)* the treetop canopy walkway.

### 2.4. Leaf sampling and biochemistry measurements

#### 2.4.1. Samples for building the EWT estimation model

Eighty-four leaf samples were collected randomly from various trees in the plot. The priority in sampling leaves for the EWT estimation model was to ensure a representative and broad sample of species, leaf types and EWT. Samples were collected from low branches in the canopy bottom that were accessible from ground using a tree pruner, and also from the canopy top, which was accessible using the treetop canopy walkway. The canopy top leaf samples predominantly represented sun leaves, while the canopy bottom leaf samples predominantly represented shade leaves. Sun leaves grow in the well-lit regions of the canopy and are usually thicker and have higher photosynthetic rates than shade leaves (Lichtenthaler et al., 1981; Terashima et al., 2005). The leaf samples included: 18 oak leaf samples, 22 beech leaf samples, 20 sycamore leaf samples, and 24 ash leaf samples. The ash leaf samples were individual leaflets of the compound leaves. Leaf sampling was carried out for each species separately. That is, the oak leaf samples were collected first, and the fresh weight (FW) of each sample was measured in field, immediately on collection, using an electronic balance (one milligram precision). The samples were then suspended in a wooden frame, positioned 8.6 m away from a tripod, and was scanned in field using the P40, followed by the P20 instrument, with a resolution of 0.8 mm at 10 m. The vertical and horizontal incidence angle effects were minimized by ensuring the wooden frame was as normal as possible to the laser beam direction. The time gap between collecting the samples and scanning them was less than fifteen minutes, and the duration of the scan was approximately five minutes for each instrument. Afterwards, the same sampling approach was repeated for each species, one after another.

The leaf samples were then transferred to the laboratory and the surface area (SA) of each leaf was obtained using Image-J 1.50i software (Schneider et al., 2012), after scanning them with a Epson Perfection photo scanner. The samples were left to dry naturally over a period of two weeks. Afterwards, they were further dried in an oven for 48 h at 60 °Celsius and were considered fully dry as no change in weight was observed when they were weighed after 40, 44, and 48 h. The dry weight (DW) of each leaf was measured and EWT was calculated as follows:

$$\text{EWT (g cm}^{-2}) = (\text{FW} - \text{DW}) / \text{SA} \quad (1)$$

Additionally, LMA of each leaf sample was calculated as follows:

$$\text{LMA (g cm}^{-2}) = \text{DW} / \text{SA} \quad (2)$$

The intensity values of each leaf sample were extracted from the scans and calibrated to apparent reflectance. NDI of reflectance was calculated for each leaf as follows:

$$\text{NDI} = (\text{P20}_\text{R} - \text{P40}_\text{R}) / (\text{P20}_\text{R} + \text{P40}_\text{R}), \quad (3)$$

where $\text{P20}_\text{R}$ and $\text{P40}_\text{R}$ are the reflectance from the P20 and P40 instruments respectively.

Reduced major axis regression was used to determine the NDI – EWT relationship for each individual species, and also for all species combined.

#### 2.4.2. Samples for validation of the EWT estimation

A total of 274 leaf samples were collected from twelve out of the thirteen trees shown in Fig. 2, as the ash tree, labelled 7, was excluded from validation as discussed in Section 2.3. Table 3 shows the number of leaf samples collected from each tree. The leaf samples were collected from two canopy layers: the canopy top layer and the canopy bottom layer. This allowed the areas sampled for validation to be explicitly identified in the TLS point cloud. The canopy top layer was 1 m above the canopy walkway level (12 m), with a depth of one meter, while the canopy bottom layer consisted of the low branches that were accessible from the ground. EWT and LMA of each leaf sample were measured following the steps described in Section 2.4.1.

**Table 3**
Details of the species, locations and numbers of the leaf samples for the EWT estimation validation. The samples from the ash tree, labelled 7, were excluded.

| Tree label | Species | Number of leaf samples | |
|---|---|---|---|
| | | Canopy top layer | Canopy bottom layer |
| 1 | Sycamore | 20 | 18 |
| 2 | Sycamore | 18 | 10 |
| 3 | Sycamore | 20 | 20 |
| 4 | Sycamore | – | 20 |
| 5 | Beech | 19 | – |
| 6 | Sycamore | 20 | – |
| 8 | Oak | – | 24 |
| 9 | Oak | 20 | – |
| 10 | Oak | 20 | – |
| 11 | Oak | 15 | – |
| 12 | Sycamore | 15 | – |
| 13 | Oak | 15 | – |
| Total number | | 182 | 92 |

### 2.5. TLS point cloud processing

#### 2.5.1. Point cloud registration and filtering

The scans collected at each scanning position were imported into Leica Cyclone (Leica Geosystems HDS). The mixed pixel filter on medium setting (default setting) was used to reduce the number of partial canopy hits. Partial hits occur when a leaf does not fully occupy the laser beam footprint, and can affect the accuracy of the TLS estimation of leaf biochemical characteristics (Eitel et al., 2010). The mixed pixel filter searched for points that have a measured range that was actually a mixture of various observed ranges. The filter then disregarded these points, as they occurred when the edge of the object partially occupied the laser footprint. The point clouds from each instrument were registered in Leica Cyclone, using the registration targets, to build the forest plot. The registered P20 scans were then aligned to the registered P40 scans. The outcome was a pair of P40/P20 aligned point clouds at each scanning positions. Points corresponding to ground and understory vegetation were removed to reduce the size of the point clouds.

A P20 point cloud was always found to have more points than the corresponding P40 point cloud, being a result of more remaining partial hits in the P20 point cloud and/or the slight difference in laser beam footprint and beam divergence between the two instruments (Table 1). Thus, for each pair of the P40/P20 aligned point clouds, an index matrix that defined the nearest neighbour in the P20 point cloud to each point in the P40 point cloud was generated by applying a nearest neighbour function in MATLAB. The index matrix was used to filter the P20 point cloud, generating a nearest neighbour point cloud containing the same number of points as the corresponding P40 point cloud. Furthermore, any pair of P40/P20 neighbour points > 3 cm apart was removed from the point cloud. The 3 cm threshold was chosen on the basis of 96% of the nearest neighbour distances being < 3 cm apart, while 99% of distances were < 6 cm apart.

#### 2.5.2. Generating the EWT point clouds

The filtered point clouds were calibrated to apparent reflectance and NDI was calculated using Eq. 3 for each pair of P40/P20 scans on a point-by-point basis. The NDI point clouds from the ten scanning positions were merged into a single point cloud that covered the entire 35 × 45 m rectangular plot. The sampled trees (Table 3) were manually extracted from the NDI point cloud. They were divided into three groups according to their species and both the species-specific and pooled NDI – EWT models (Section 3.2.1) were applied to generate the

EWT point clouds.

#### 2.5.3. Validating the EWT estimations

Visual inspection of the NDI point cloud and histogram of each tree showed that foliage NDI was clustered around 0.3, while for wood it was clustered around zero. Wood typically is expected to have higher shortwave infrared reflectance than green foliage, as it contains less moisture, while their near infrared reflectance is expected to be similar at the wavelength used in this study (808 nm). This caused the lower NDI values of wood components. Applying the NDI – EWT estimation models (Eqs. 5 to 9), trained solely using green foliage, would then result in the majority of points corresponding to woody materials to have EWT value equal to or below zero, even if they had higher moisture in reality. The same applies to noise points, resulted from wrongly assigned nearest neighbours, that is, a full hit being assigned to a partial hit, resulting in a very low or a very high NDI value. As the focus of this study was to estimate EWT of foliage only, a threshold of zero was used to disregard the points corresponding to wood and noise. Afterwards, using visual inspection, points that clearly corresponded to wood, being part of the trunk or primary branches, but were wrongly classified as leaves, were manually removed. In addition, it was possible to visually identify and remove many of the points corresponding to lateral branches. However, it was not possible to identify and remove smaller branches and twigs. Additionally, a Gaussian distribution was fitted to the EWT histogram and a threshold equal to twice the mean value was applied to filter points with very high EWT (Fig. 3).

The layers from which the leaf samples were collected were extracted from each individual tree point cloud. The estimated EWT of each layer was compared to the actual EWT of the leaf samples collected from that layer and the relative error was calculated as follows:

$$E\% = ((\text{Estimated EWT} - \text{Actual EWT}) / \text{Actual EWT}) \times 100 \quad (4)$$

The EWT point cloud of each tree was divided into a number of horizontal layers, each 1 m deep. EWT of each layer was plotted against the corresponding height to produce the EWT vertical profile of the tree. The EWT vertical profiles were produced from the EWT point clouds generated using the pooled EWT estimation model (Eq. 9).

## 3. Results and discussion

### 3.1. Leaf internal structure effects on NDI

#### 3.1.1. The effects of N and LMA on the NDI

Changing N significantly affected the leaf reflectance in the visible, near infrared and shortwave infrared regions of the electromagnetic spectrum, with higher values of N leading to an increasing reflectance (Fig. 4a). On the other hand, LMA affected the leaf reflectance in the near and shortwave infrared regions only, with higher values of LMA resulting in a lower leaf reflectance (Fig. 5a). The 808 nm and 1550 nm wavelengths showed similar sensitivity to the change in N and LMA, and combining them in the NDI minimized but did not entirely normalize these effects (Fig. 4b and Fig. 5b). A leaf with a more compact mesophyll structure would have a slightly higher NDI than a leaf with a more differentiated structure, even if they both had an identical EWT. On the other hand, a leaf with respectively lower LMA would have a slightly lower NDI than a leaf with higher LMA that has the same EWT value and area.

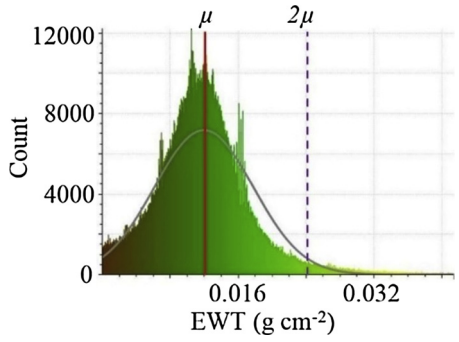


**Fig. 3.** Example of using the mean (μ) of the fitted EWT histogram Gaussian distribution to remove the noise by applying a threshold equal to 2μ (purple) (For interpretation of the references to colour in this figure legend, the reader is referred to the web version of this article).

#### 3.1.2. The effects of N and LMA on the NDI – EWT relationship

An increase in N resulted in a shift in the trendline of the NDI – EWT relationship downwards (Fig. 6a), with the effects of N appearing to be more significant for higher EWT values. On the other hand, an increase in LMA caused the trendline of the NDI – EWT relationship to be shifted up (Fig. 6b), with the effects being slightly more significant for lower EWT values. It is worth mentioning that although N and LMA were considered uncorrelated parameters in the simulations, for the sake of studying their effects on NDI individually, they are highly correlated in reality. N is correlated to the Specific Leaf Area (SLA), defined as the leaf surface area divided by the leaf dry mass, and an increase in SLA leads to a decrease in N (Jacquemoud and Baret, 1990). Thus, N is also highly correlated to LMA, as LMA is the reciprocal of SLA. A thinner leaf would frequently have a lower N value than a thicker leaf, and correspondingly a lower LMA value. Although the PROSPECT simulations revealed that both N and LMA individually affect NDI, when their effects are combined they would be minimized as they would cancel each other out (Figs. 4b and 5b). Thus, a change in NDI would be mainly caused by a change in EWT, with some remaining minor influence of N and LMA.

### 3.2. Leaf sampling and biochemistry measurements

#### 3.2.1. Samples for building the EWT estimation model

For each individual species, moderate correlation was observed between NDI and EWT ($R^2$ = 0.55, 0.57, 0.59 and 0.68 for the beech, ash, oak and sycamore species respectively). Some differences in the slope and intercept of the NDI – EWT relationship were observed between the different species (Fig. 7). This can be a result of the remaining effects of the leaf internal structure on the NDI, as PROSPECT simulations revealed that NDI can minimize but not entirely normalize such effects (Section 3.1). The species-specific NDI – EWT relationships can be described as:

$$EWT\ (g\ cm^{-2}) = 0.0488 \times NDI - 0.0016, \text{ for the sycamore species} \quad (5)$$

$$EWT\ (g\ cm^{-2}) = 0.0553 \times NDI - 0.0031, \text{ for the oak species} \quad (6)$$

$$EWT\ (g\ cm^{-2}) = 0.0327 \times NDI - 0.0002, \text{ for the beech species} \quad (7)$$

$$EWT\ (g\ cm^{-2}) = 0.0534 \times NDI - 0.0032, \text{ for the ash species} \quad (8)$$

The species-specific relationships for beech and oak were based on a narrow EWT range. A linear model was therefore fitted to all the leaf samples combined ($R^2$ = 0.94) (Fig. 7) to provide an improved calibration equation. However, it is acknowledged that there remains a gap in the EWT values, between 0.0055 g/cm$^2$ and 0.008 g/cm$^2$, thus the high correlation can potentially be misleading. More leaf samples are needed in future work in order to fill this gap in the model, but the consistency of trends between the general and individual species models give confidence it is suitable for application at canopy scale. The model can be described as:

$$EWT\ (g\ cm^{-2}) = 0.0579 \times NDI - 0.0039 \quad (9)$$

#### 3.2.2. Samples for validation of the EWT estimation

The average EWT of all leaf samples collected from the canopy top

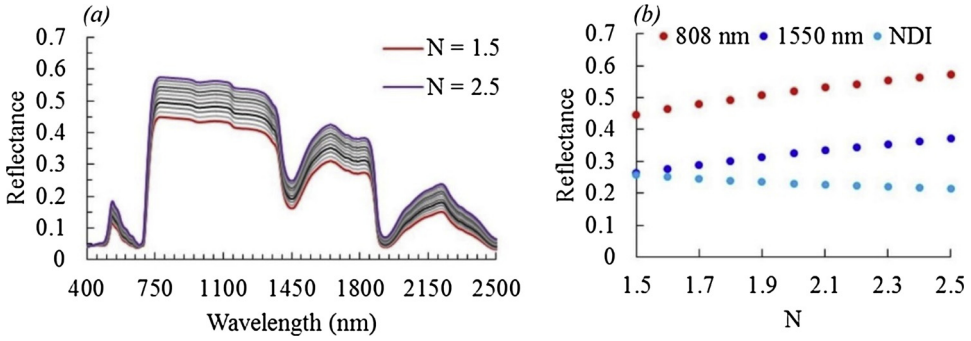


**Fig. 4.** *(a)* Effects of N on the leaf reflectance, and *(b)* effects of N on 808 nm wavelength, 1550 nm wavelength, and NDI.

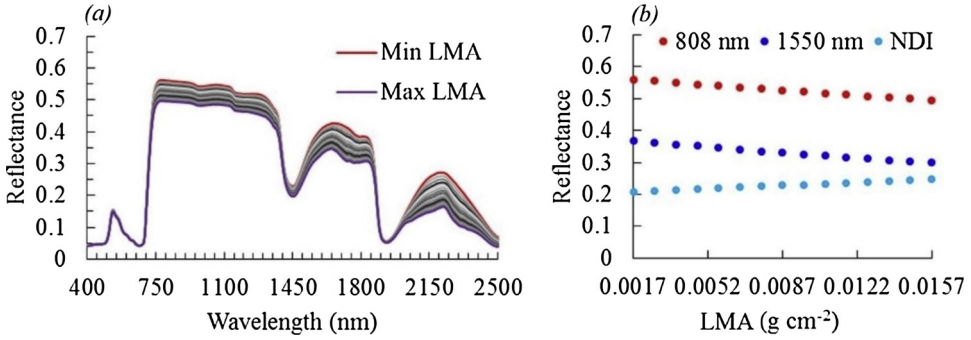


**Fig. 5.** *(a)* Effects of LMA on the leaf reflectance and *(b)* effects of LMA on 808 nm wavelength, 1550 nm wavelength and NDI.

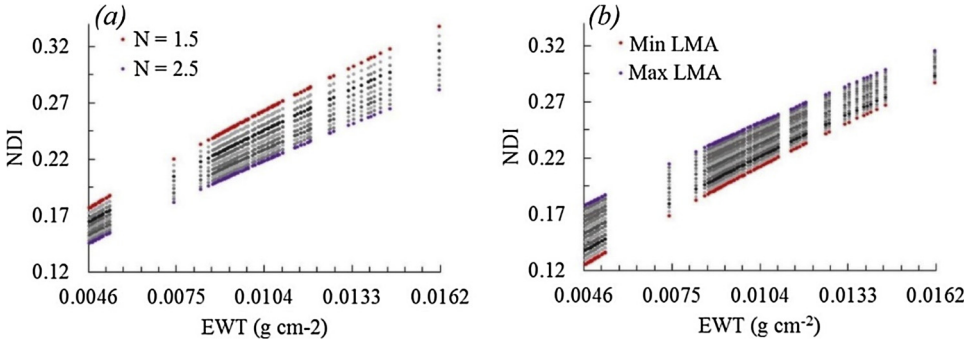


**Fig. 6.** *(a)* Effects of N on the NDI – EWT relationship and *(b)* effects of LMA on the NDI – EWT relationship.

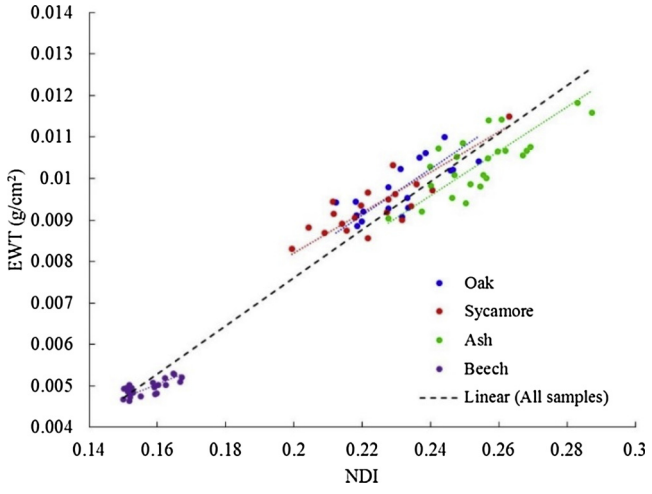


**Fig. 7.** NDI – EWT relationships for individual species and for all the samples combined.

layer was 20% higher than that of the leaf samples collected from the canopy bottom layer (Fig. 8). This revealed a vertical heterogeneity in EWT within canopies and agreed to the findings of Zhu et al. (2017) and Elsherif et al. (2018), although these studies dealt only with individual small trees in indoor experiments. In addition, LMA of leaf samples from the canopy top layer was 42% higher than that of the canopy bottom layer, suggesting that the observed higher EWT in the canopy top was caused by the leaves having higher LMA, increasing their ability to hold moisture. To further investigate, the relationship between EWT and LMA for all leaf samples was studied (Fig. 9), revealing that EWT and LMA were highly correlated ($R^2$ = 0.92, 0.61, 0.60 and 0.63 for beech, ash, oak and sycamore respectively), and that the relationship between EWT and LMA was species-specific. Additionally, studying the EWT – LMA relationship within each species revealed some differences between the individual trees (Fig. 10).

The lowest EWT observed was 0.0046 g/cm$^2$, while the highest was 0.0145 g/cm$^2$. According to PROSPECT simulations results (Section 3.1), this change in EWT would cause a 79% increase in NDI, assuming constant values of N and LMA. On the other hand, the lowest LMA observed was 0.0014 g/cm$^2$ and the highest was 0.0063 g/cm$^2$. Such a change in LMA, assuming constant EWT and N, would cause only a 7%

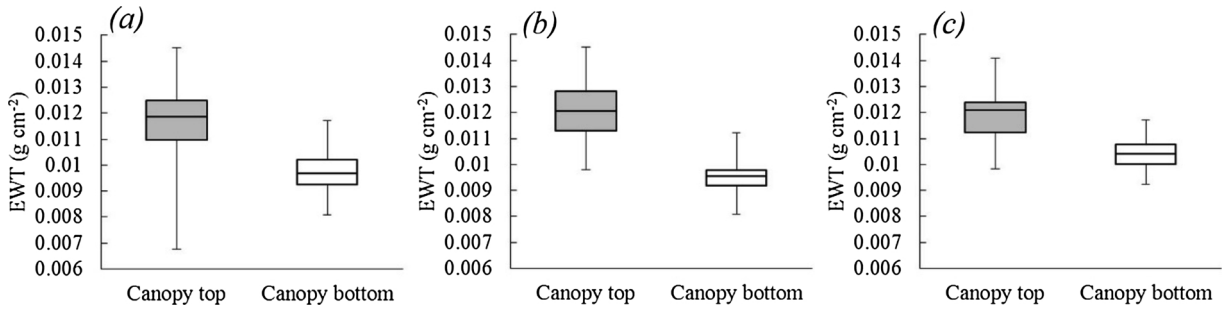


**Fig. 8.** A boxplot of the EWT of the leaf samples in canopy top and canopy bottom layers: *(a)* all leaf samples combined, *(b)* sycamore, and *(c)* oak. The whiskers are the minimum and maximum values.

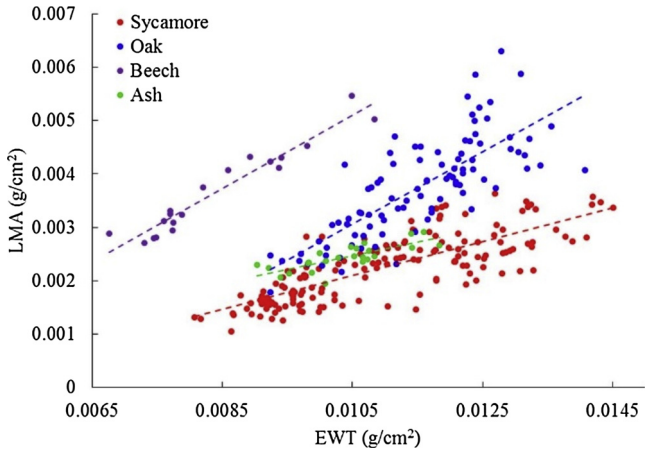


**Fig. 9.** The EWT – LMA relationships of the leaf samples from the four species.

increase in NDI. For N, assuming that the leaves covered the whole range between 1.5 and 2.5, changing N, while EWT and LMA remained constant, would result in a 17% reduction in NDI. This further showed that NDI was mainly affected by the change in EWT.

### 3.3. EWT point clouds

The Root Mean Square Error (RMSE) of the point cloud registration, reported by Leica Cyclone, was 3 mm for each instrument separately. As the scans were conducted at a resolution of 3 mm at 10 m, the registration accuracy was considered sufficient. The RMSE of the registration of the P20 point clouds to the P40 point clouds was 1 mm. The high accuracy was a result of the similarities between the two instruments in terms of their scanning mechanism and laser beam exit location, and also a result of the similar scanning geometry. Another key factor was the absence of wind. Scanning in more windy conditions would be expected to significantly reduce the registration accuracy. The high registration accuracy allowed the generation of 3D EWT point clouds, as shown in Figs. 11 and 12.

The point clouds revealed a significant difference between the leaf and wood EWT, showing some potential of using the 3D EWT distribution in separating the leaf from the wood using zero EWT as a separation threshold. However, testing this method revealed that many points that clearly corresponded to wood (*e.g.* trunk, primary branches, lateral branches) had above zero EWT, and thus were mistakenly classified as leaves. Attempting to filter these points using a higher threshold resulted in removing points clearly corresponding to leaves. Thus, these points had to be removed manually, which renders this method impractical at plot scale. In addition, it was not possible to visually identify and manually remove misclassified points that corresponded to small branches and twigs. Additionally, numerous points corresponding to leaves were also classified as wood, as they had below zero EWT. This could be a result of wrongly assigned nearest neighbours, as discussed in Section 2.5.3. It was possible to filter these points using the statistical outlier removal tool in the CloudCompare v. 2.6.2 software, as they were sparse points in comparison to the very dense points in the trunk and branches. However, this method may also filter small branches and twigs, and as no field measurements were conducted to validate this leaf-wood separation approach, it was not possible to determine its accuracy.

### 3.4. Validating the EWT estimations

Comparing the estimated EWT to the actual EWT from the leaf samples revealed a relative error of 7.7% on average in the EWT estimations for the species-specific models and 6.3% for the pooled model. Table 4 summarizes all the observed errors. The largest observed error

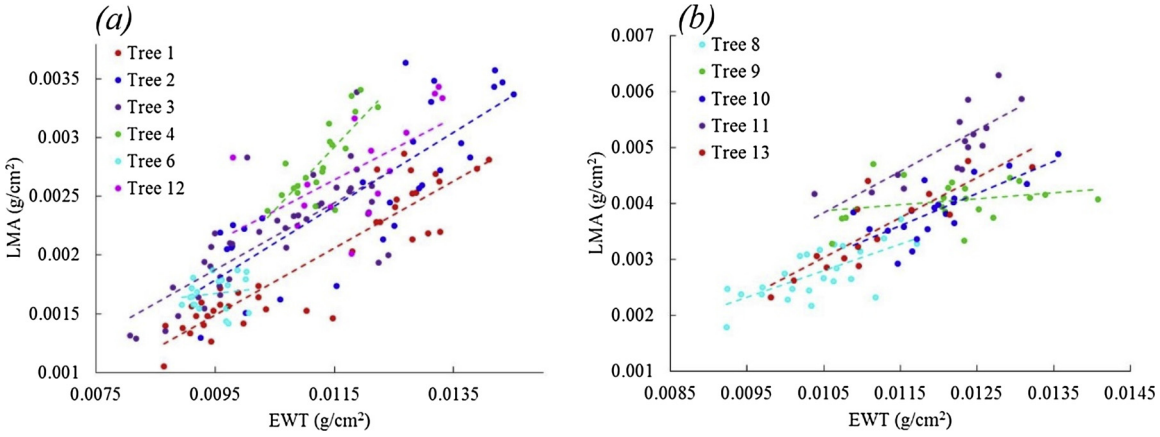


**Fig. 10.** The EWT – LMA relationships of the individual trees: *(a)* sycamore and *(b)* oak.


**Fig. 11.** The 3D EWT distribution of the sampled trees.

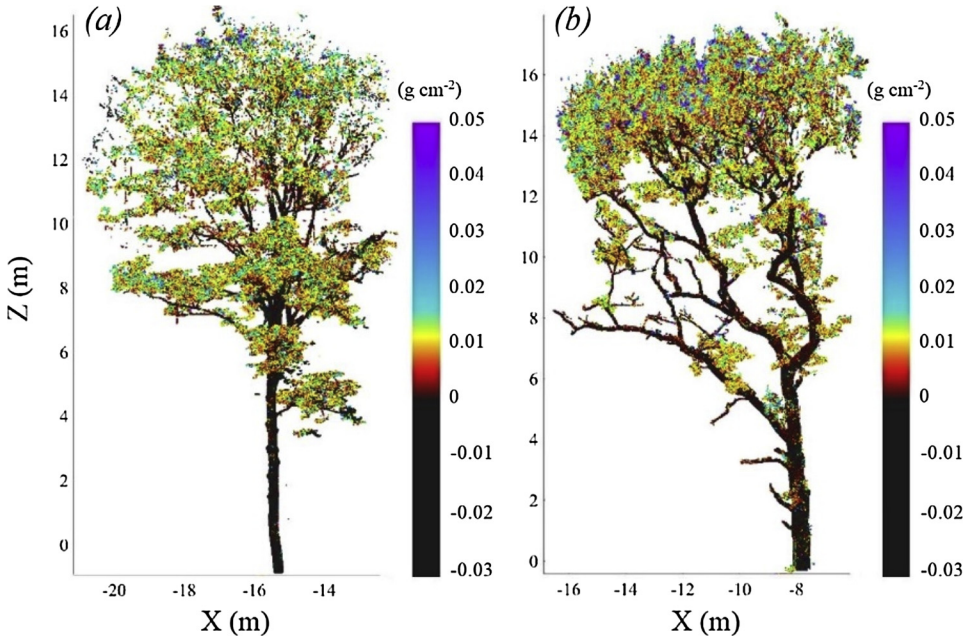


**Fig. 12.** Examples of the 3D EWT distribution of individual trees: (a) Sycamore tree, labelled (6), and (b) Oak tree, labelled (11).

for the species-specific models was -21% for the beech tree. This high error can be a result of the narrow range of EWT in the leaf samples used to build the EWT estimation model, which was insufficient to accurately determine the slope and intercept of the NDI – EWT relationship. All the remaining errors were < 10%, except for the errors obtained in the canopy top layer in sycamore trees number 2 and 12, and in the canopy bottom layer in oak tree number 8. When the pooled model was used, the error in the EWT estimation for the beech tree dropped to -2.8%, further showing that the species-specific model of beech was inaccurate. The errors in sycamore trees number 2 and 12 increased, with the errors being higher than those observed in the remaining sycamore trees. As EWT was underestimated, this suggested lower NDI values, which can be a result of the remaining effects of the leaf internal structure on the NDI, if leaf samples from these two trees were thicker than the leaves used to build the EWT estimation model, according to PROSPECT simulations. On the other hand, the error in the EWT estimation in oak tree 8 dropped when the pooled model was used, but remained higher than the errors observed in the remaining oak trees. The overestimation of EWT suggested that leaf samples collected from that specific tree were thinner than the leaf samples used to build the EWT estimation model.

The observed EWT estimation errors showed the possibility of using a pooled NDI – EWT model to successfully estimate EWT in a mixed forest plot without needing a NDI – EWT estimation model for each individual species. Using a pooled EWT model can then be more applicable as it does not require prior tree species classification. However, further experiments that include measuring leaf thickness are still needed to better understand the source of the high errors observed in some trees.

**Table 4**
A summary of the EWT estimation errors in the twelve trees, for the canopy top and bottom layers. The signs of the errors were ignored while calculating the average and total errors.

| Tree | Species | Relative error in EWT estimations | | | |
|---|---|---|---|---|---|
| | | Species-specific models | | Pooled model | |
| | | Canopy top | Canopy bottom | Canopy top | Canopy bottom |
| 1 | Sycamore | −5.9% | 9.2% | −5.3% | 7.2% |
| 2 | Sycamore | −13.5% | 6% | −13.5% | 4.3% |
| 3 | Sycamore | −2.5% | 6.9% | −2.7% | 4.3% |
| 4 | Sycamore | – | 9.3% | – | 7.3% |
| 5 | Beech | −21% | – | −2.8% | – |
| 6 | Sycamore | −0.7% | – | −1% | – |
| 8 | Oak | – | 12.5% | – | 10.2% |
| 9 | Oak | 8% | – | 6.7% | – |
| 10 | Oak | 3.7% | – | 2.1% | – |
| 11 | Oak | −0.6% | – | −2.4% | – |
| 12 | Sycamore | −12% | – | −13.3% | – |
| 13 | Oak | −3% | – | −5.4% | – |
| Average error | | 7.1% | 8.8% | 5.5% | 6.7% |
| Total error | | 7.7% | | 6.3% | |

### 3.5. EWT vertical profiles

The EWT vertical profiles (Fig. 13) revealed a vertical variation in the EWT distribution in all twelve trees, agreeing to the leaf sampling results (Section 3.2.2). Fig. 13 also shows the advantage of using TLS data in mapping the EWT in forest plots over the destructive sampling approach. TLS can estimate EWT in all canopy layers, which requires tree climbers and extensive destructive sampling to be achieved using traditional approaches. Assuming that the leaves in the top part of the canopy were sun leaves, and those in the bottom were shade leaves, the vertical profiles of EWT showed a gradual transition between sun leaves and shades leaves, with sun leaves having higher EWT, and correspondingly higher LMA, than shade leaves.

All trees had higher EWT in the upper canopy than in the shaded lower canopy. This concurred with the findings of Zhu et al. (2017); Elsherif et al. (2018) and Gara et al. (2018), all reporting higher EWT in the canopy top than the canopy bottom in variety of species. The upper canopy in all trees had an average of 24.2% more EWT than the lower canopy. However, the errors presented in Table 4 showed that the EWT estimation models overestimated the EWT in the canopy bottom layer and, in most cases, underestimated the EWT in the canopy top layer, suggesting that the actual difference between EWT of upper and lower canopy can be higher than 24.2%. The highest observed variation in EWT was in the beech tree, labelled (5), where EWT in the upper canopy was 44% higher than the bottom canopy. The lowest variation was observed in the oak tree, labelled (10), where EWT was 13.6% higher in the upper canopy than in the lower. Similarities were observed in the vertical profiles of the sycamore trees, with the upper canopy layer having an average of 20% higher EWT than the lower canopy. The vertical profile of the beech tree was more distinctive. The vertical profiles of the oak trees showed some variations from each other, with EWT being 25.4% higher in upper canopy than in lower canopy, which suggested that the EWT vertical profile can vary within a species, depending on each individual tree structure.

As discussed in Section 3.2.2, EWT and LMA were found to be highly correlated. Thus, EWT vertical profiles shown in Fig. 13 also reflected the vertical variation in LMA within canopies. Furthermore, the EWT – LMA relationships can be used to derive LMA vertical profiles and 3D distributions, based on the generated 3D EWT point clouds. When the pooled EWT – LMA relationships, shown in Fig. 9, were tested to produce LMA vertical profiles, large errors were observed in some trees, as large as 40%, especially in the canopy bottom layers, although the samples used for validation were the same samples used to build the EWT – LMA models. When tree-specific models were used (Fig. 10), the errors dropped. The average error in the LMA estimation was 7.1%, whilst the errors in each tree were less than 10%, except for trees 1 and 3 canopy bottom layers (18% and 13.4% respectively). Although this showed the potential of using EWT to generate 3D estimates of LMA, the method seemed to be applicable at individual tree level only and applying it at plot level can be challenging.

## 4. Conclusions

The main focus of this study was to investigate the possibility of using dual-wavelength TLS to generate 3D EWT estimations at canopy level in a mixed forest plot. The NDI of a near infrared wavelength (808 nm) and a shortwave infrared wavelength (1550 nm), employed in the Leica P20 and P40 commercial TLS instruments respectively, was used to map EWT in 3D at canopy level in a mixed deciduous forest plot in Wytham Woods, Oxford, UK. PROSPECT simulations were carried out to study the ability of the NDI to normalize the leaf internal structure effects and revealed that NDI can minimize such effects. Such ability allowed the using of NDI to estimate EWT at canopy level without the need for calibration for the variation in the leaf internal structure within each individual species or between different species.

At leaf level, moderate correlation was observed between NDI and EWT across four broadleaf tree species: oak, sycamore, beech and ash. It was also possible to fit a pooled EWT estimation model that combined all species, but more leaf samples still need to be added to the model to fill the gap in the low EWT region of the model. At canopy level, it was possible to achieve a high registration accuracy for the point clouds, despite the difference in the laser beam footprint and beam divergence between the two instruments. This was a result of the similarity in the chassis of the instruments and their laser beam exit locations, in addition to the similarity in the scan geometry. NDI was successfully used to generate 3D estimations of EWT in the scanned forest plot, using species-specific models in addition to a pooled EWT model, with a relative error of 7.7% and 6.3% in the EWT estimation respectively. The generated 3D distributions of EWT revealed some vertical heterogeneity in all the sampled trees. All the trees were found to have higher EWT in the canopy top than the canopy bottom, with EWT gradually becoming lower as we move down the canopy. Such variation in EWT can be a result of the leaves in the top of the canopy, predominantly sun leaves, having higher LMA than shaded leaves in the bottom of the canopy, as EWT and LMA were found to be highly correlated. The observed EWT vertical variation in the forest plot may affect the estimation of EWT using passive optical space or airborne sensors, because measurements from such instruments will be dominated by the canopy top, which, according to this study, has higher EWT than the lower layers in the canopy. However, the vertical profile of EWT still needs to be investigated across additional species and in different sites.

This study showed the potential of using commercially-available TLS instruments to provide important insights into the EWT distribution within forest canopies, by mapping the EWT at canopy level in 3D. The proposed approach can serve as a powerful tool to study the variation of EWT within the canopy and between different species, can provide high spatial and temporal EWT estimations, independent of the cloud coverage and solar illumination, and can estimate EWT predawn and midday. Additionally, if coupled with optical spaceborne or airborne remote sensing data, the 3D EWT estimates can result in a better understanding of the effects of the woody materials, soil, and understory vegetation on the optical remote sensing estimation of EWT. The 3D EWT estimates can also be implemented in 3D radiative transfer models to investigate the effects of the EWT vertical variation on the optical sensor measured reflectance. In addition, the technique could allow characterisation of whole-tree leaf water status and total water content, if total leaf area can be derived. TLS has shown potential for estimation of LAI at stand and canopy scales (Antonarakis et al., 2010; Zheng et al., 2013) and combining these methods could provide new insights into

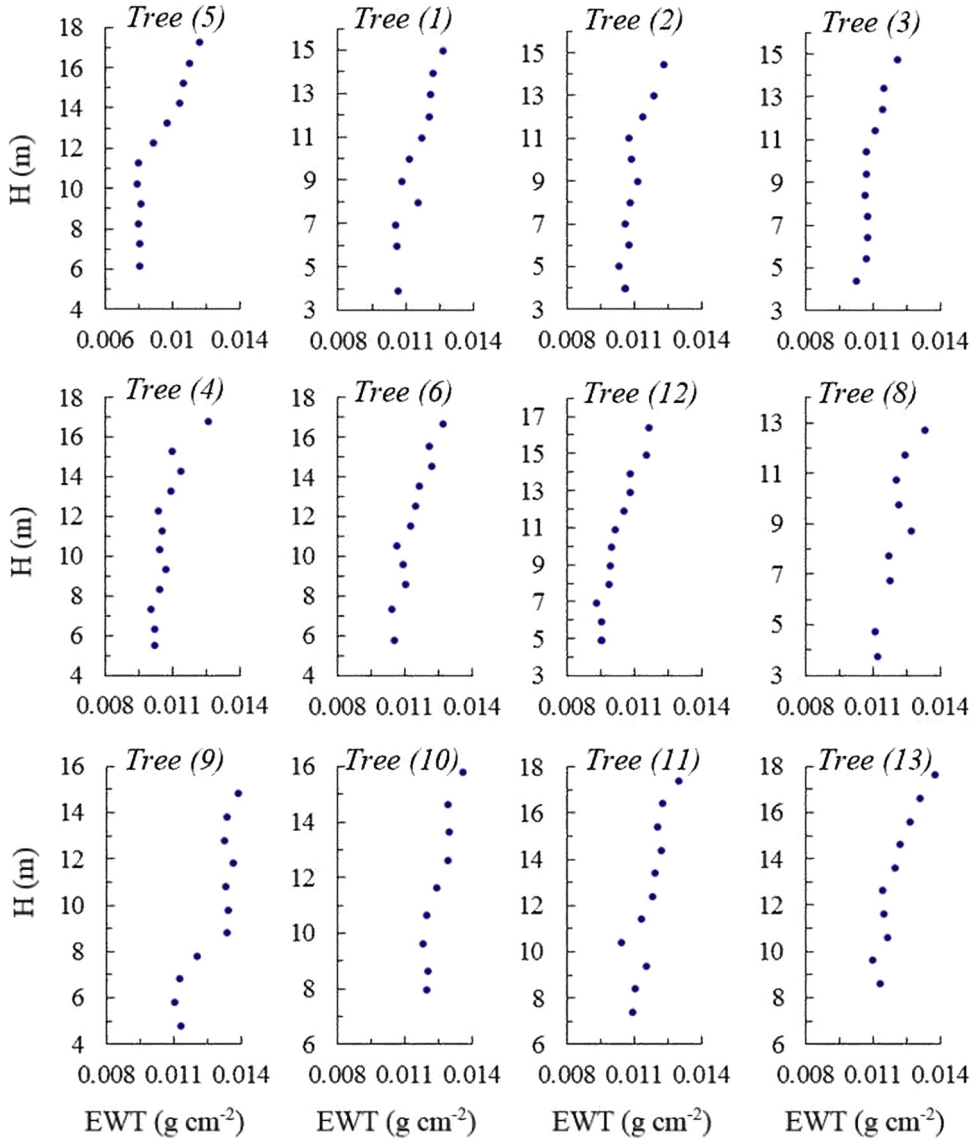


**Fig. 13.** The EWT vertical profiles. Tree (5) is beech, trees (1, 2, 3, 4, 6 and 12) are sycamore and trees (8, 9, 10, 11 and 13) are oak.

forest health and functioning.

## 5. Declaration of Competing Interest

None.

## Authors' contributions

Ahmed Elsherif planned and carried out the experiments and data collection, wrote the processing codes and analysed the data, as well as drafting the manuscript. Rachel Gaulton and Jon Mills contributed to planning the experiments, interpretation of results and helped draft and edit the manuscript. Alexander Shenkin contributed in the interpretation of the results and in revising and editing the manuscript. Yadvinder Malhi contributed in the interpretation of the results. All authors gave final approval for publication.

## Acknowledgements

The authors would like to thank the Natural Environment Research Council (NERC) Centre for Earth Observation for providing the Spectralon panels used in the calibration. We are also grateful to Leica Geosystems UK for loan of the P40 scanner used in the experiments. We also would like to thank Nigel Fisher for his support at Wytham Woods.

## Funding

This work was funded by the Ministry of Higher Education, Egypt, represented by the Egyptian Cultural and Educational Bureau in London, UK, as a part of Ahmed Elsherif PhD scholarship.

## Appendix A

SphereOptics® spectralon panels (Table A1) were used to repeat the calibration work described in (Elsherif et al., 2018) and update the intensity calibration models.

The polynomial functions that describe the range effects for the P40 instrument:

**Table A1**
Spectralon panels' true reflectance at 1550 nm and 808 nm wavelengths.

| Spectralon | 5% | 20% | 50% | 90% | 95% |
|---|---|---|---|---|---|
| P40 (1550 nm) | 4.7% | 24.2% | 41.8% | 90.2% | 94.7% |
| P20 (808 nm) | 4.5% | 22.6% | 43.5% | 92.2% | 96.1% |

$$I_P = 0.0004 \times Ra^3 - 0.0061 \times Ra^2 + 0.0294 \times Ra - 0.0089, \text{ for } Ra < 5\,m \quad (A.1)$$

$$I_P = (-1.2 \times 10^{-10}) \times Ra^6 + (1.3 \times 10^{-8}) \times Ra^5 - (4.98 \times 10^{-7}) \times Ra^4 + (4.5 \times 10^{-6}) \times Ra^3 + (1.1 \times 10^{-4}) \times Ra^2 - 0.0022 \times Ra + 0.0444, \text{ for } Ra > 5\,m \quad (A.2)$$

The polynomial functions that describe the range effects for the P20 instrument:

$$I_P = -0.0014 \times Ra^2 + 0.0123 \times Ra + 0.0150, \text{ for } Ra < 5\,m \quad (A.3)$$

$$I_P = (5.5 \times 10^{-10}) \times Ra^6 - (7.5 \times 10^{-8}) \times Ra^5 + (4.1 \times 10^{-6}) \times Ra^4 - (1.1 \times 10^{-4}) \times Ra^3 + 0.0017 \times Ra^2 - 0.0122 \times Ra + 0.0719, \text{ for } Ra > 5\,m \quad (A.4)$$

where $I_P$ is the intensity from the polynomial function at a range Ra.

The intensity – reflectance relationships for the P40 instrument:

$$P40_R = 53.861 \times P40_I^2 + 8.992 \times P40_I + 0.0003, \text{ for } Ra < 5\,m \quad (A.5)$$

$$P40_R = 45.553 \times P40_I^2 + 9.307 \times P40_I + 0.0044, \text{ for } Ra > 5\,m \quad (A.6)$$

where $P40_R$ is the reflectance corresponding to a $P40_I$ intensity value.

The intensity – reflectance relationships for the P20 instrument:

$$P20_R = 45.942 \times P20_I^2 + 8.490 \times P20_I + 0.002, \text{ for } Ra < 5\,m \quad (A.7)$$

$$P20_R = 40.981 \times P20_I^2 + 9.109 \times P20_I + 0.0052, \text{ for } Ra > 5\,m \quad (A.8)$$

where $P20_R$ is the reflectance corresponding to a $P20_I$ intensity value.

The near-range intensity – reflectance models account for the effects of the near-distance intensity reducer in both instruments.

## References


Ali, A.M., Darvishzadeh, R., Skidmore, A.K., Duren, Iv., 2016. Effects of canopy structural variables on retrieval of leaf dry matter content and specific leaf area from remotely sensed data. Journal of Selected Topics in Applied Earth Observations and Remote Sensing 9, 898–909.

Améglio, T., Archer, P., Cohen, M., Valancogne, C., Daudet, F.-a., Dayau, S., Cruiziat, P., 1999. Significance and limits in the use of predawn leaf water potential for tree irrigation. Plant Soil 207, 155–167.

Antonarakis, A.S., Richards, K.S., Brasington, J., Muller, E., 2010. Determining leaf area index and leafy tree roughness using terrestrial laser scanning. Water Resour. Res. 46.

Anttila, K., Hakala, T., Kaasalainen, S., Kaartinen, H., Nevalainen, O., Krooks, A., Kukko, A., Jaakkola, A., 2016. Calibrating laser scanner data from snow surfaces: correction of intensity effects. Cold Reg. Sci. Technol. 121, 52–59.

Baret, F., Guyot, G., 1991. Potentials and limits of vegetation indices for LAI and APAR assessment. Remote Sens. Environ. 35, 161–173.

Blaskow, R., Schneider, D., 2014. Analysis and correction of the dependency between laser scanner intensity values and range. The International Archives of Photogrammetry, Remote Sensing and Spatial Information Sciences 40, 107–112.

Bonan, G.B., 2008. Forests and climate change: forcings, feedbacks, and the climate benefits of forests. Science 320, 1444–1449.

Carter, G.A., 1993. Responses of leaf spectral reflectance to plant stress. Am. J. Bot. 80, 239–243.

Ceccato, P., Flasse, S., Tarantola, S., Jacquemoud, S., Grégoire, J.-M., 2001. Detecting vegetation leaf water content using reflectance in the optical domain. Remote Sens. Environ. 77, 22–33.

Ciganda, V., Gitelson, A., Schepers, J., 2008. Vertical profile and temporal variation of chlorophyll in maize canopy: quantitative crop vigor indicator by means of reflectance-based techniques. Agron. J. 100, 1409–1417.

Clevers, J.G.P.W., Kooistra, L., Schaepman, M.E., 2010. Estimating canopy water content using hyperspectral remote sensing data. Int. J. Appl. Earth Obs. Geoinf. 12, 119–125.

Colombo, R., Meroni, M., Marchesi, A., Busetto, L., Rossini, M., Giardino, C., Panigada, C., 2008. Estimation of leaf and canopy water content in poplar plantations by means of hyperspectral indices and inverse modelling. Remote Sens. Environ. 112 (4), 1820–1834.

Danson, F.M., Bowyer, P., 2004. Estimating live fuel moisture content from remotely sensed reflectance. Remote Sens. Environ. 92, 309–321.

Danson, F.M., Steven, M.D., Malthus, T.J., Clark, J.A., 1992. High-spectral resolution data for determining leaf water content. Int. J. Remote Sens. 13, 461–470.

Dash, J.P., Watt, M.S., Pearse, G.D., Heaphy, M., Dungey, H.S., 2017. Assessing very high resolution UAV imagery for monitoring forest health during a simulated disease outbreak. Isprs J. Photogramm. Remote. Sens. 131, 1–14.

Eitel, J.U.H., Vierling, L.A., Long, D.S., 2010. Simultaneous measurements of plant structure and chlorophyll content in broadleaf saplings with a terrestrial laser scanner. Remote Sens. Environ. 114, 2229–2237.

Elsherif, A., Gaulton, R., Mills, J., 2018. Estimation of vegetation water content at leaf and canopy level using dual-wavelength commercial terrestrial laser scanners. Interface Focus 8.

Feret, J.-B., François, C., Asner, G.P., Gitelson, A.A., Martin, R.E., Bidel, L.P.R., Ustin, S.L., Le Maire, G., Jacquemoud, S., 2008. PROSPECT-4 and 5: advances in the leaf optical properties model separating photosynthetic pigments. Remote Sens. Environ. 112, 3030–3043.

Ferretti, M., 1997. Forest health assessment and monitoring–issues for consideration. Environ. Monit. Assess. 48, 45–72.

Gara, T.W., Darvishzadeh, R., Skidmore, A.K., Wang, T., 2018. Impact of vertical canopy position on leaf spectral properties and traits across multiple species. Remote Sens. (Basel) 10, 346.

Gaulton, R., Danson, F.M., Ramirez, F.A., Gunawan, O., 2013. The potential of dual-wavelength laser scanning for estimating vegetation moisture content. Remote Sens. Environ. 132, 32–39.

Hancock, S., Gaulton, R., Danson, F.M., 2017. Angular reflectance of leaves with a dual-wavelength terrestrial lidar and its implications for leaf-bark separation and leaf moisture estimation. Ieee Trans. Geosci. Remote. Sens. 55 (3084).

Höfle, B., Pfeifer, N., 2007. Correction of laser scanning intensity data: data and model-driven approaches. Isprs J. Photogramm. Remote. Sens. 62, 415–433.

Jacquemoud, S., Baret, F., 1990. PROSPECT—a model of leaf optical-properties spectra. Remote Sens. Environ. 34, 75–91.

Junttila, S., Sugano, J., Vastaranta, M., Linnakoski, R., Kaartinen, H., Kukko, A., Holopainen, M., Hyyppä, H., Hyyppä, J., 2018. Can leaf water content Be estimated using multispectral terrestrial laser scanning? A case study with Norway spruce seedlings. Front. Plant Sci. 9, 299.

Junttila, S., Vastaranta, M., Liang, X., Kaartinen, H., Kukko, A., Kaasalainen, S., Holopainen, M., Hyyppä, H., Hyyppä, J., 2016. Measuring leaf water content with dual-wavelength intensity data from terrestrial laser scanners. Remote Sens. (Basel) 9, 8.

Jutzi, B., Gross, H., 2009. Normalization of LiDAR intensity data based on range and surface incidence angle. ISPRS International Archives of the Photogrammetry, Remote Sensing and Spatial Information Sciences 38, 213–218.
Kaasalainen, S., Jaakkola, A., Kaasalainen, M., Krooks, A., Kukko, A., 2011. Analysis of incidence angle and distance effects on terrestrial laser scanner intensity: search for correction methods. Remote Sens. (Basel) 3, 2207–2221.
Krooks, A., Kaasalainen, M., Hakala, T., Nevalainen, O., 2013. Correction of intensity incidence angle effect in terrestrial laser scanning. Isprs Ann. Photogramm. Remote. Sens. Spat. Inf. Sci. 145–150 II-5/W2.
Lewis, S.L., Edwards, D.P., Galbraith, D., 2015. Increasing human dominance of tropical forests. Science 349, 827–832.
Lichtenthaler, H.K., Buschmann, C., Döll, M., Fietz, H.J., Bach, T., Kozel, U., Meier, D., Rahmsdorf, U., 1981. Photosynthetic activity, chloroplast ultrastructure, and leaf characteristics of high-light and low-light plants and of sun and shade leaves. Photosyn. Res. 2, 115–141.
Lisar, S.Y.S., Motafakkerazad, R., Hossain, M.M., Rahman, I.M.M., 2012. Water stress in plants: causes, effects and responses. Water stress: InTech.
Liu, S., Peng, Y., Wei, D., Le, Y., Li, L., 2015. Remote estimation of leaf and canopy water content in winter wheat with different vertical distribution of water-related properties. Remote Sens. (Basel) 7, 4626–4650.
McMahon, S.M., Bebber, D.P., Butt, N., Crockatt, M., Kirby, K., Parker, G.G., Riutta, T., Slade, E.M., 2015. Ground based LiDAR demonstrates the legacy of management history to canopy structure and composition across a fragmented temperate woodland. For. Ecol. Manage. 335, 255–260.
Meentemeyer, R.K., Anacker, B.L., Mark, W., Rizzo, D.M., 2008. Early detection of emerging forest disease using dispersal estimation and ecological niche modeling. Ecol. Appl. 18, 377–390.
Millar, C.I., Stephenson, N.L., 2015. Temperate forest health in an era of emerging megadisturbance. Science 349, 823–826.
Morecroft, M.D., Taylor, M.E., Ellwood, S.A., Quinn, S.A., 2001. Impacts of deer herbivory on ground vegetation at Wytham Woods, central England. Forestry 74, 251–257.
Pan, Y., Birdsey, R.A., Fang, J., Houghton, R., Kauppi, P.E., Kurz, W.A., Phillips, O.L., Shvidenko, A., Lewis, S.L., Canadell, J.G., 2011. A large and persistent carbon sink in the world's forests. Science 1201609.
Pasqualotto, N., Delegido, J., Van Wittenberghe, S., Verrelst, J., Rivera, J.P., Moreno, J., 2018. Retrieval of canopy water content of different crop types with two new hyperspectral indices: water Absorption Area Index and Depth Water Index. Int. J. Appl. Earth Obs. Geoinf. 67, 69–78.
Penasa, L., Franceschi, M., Preto, N., Teza, G., Polito, V., 2014. Integration of intensity textures and local geometry descriptors from Terrestrial Laser Scanning to map chert in outcrops. Isprs J. Photogramm. Remote. Sens. 93, 88–97.
Peñuelas, J., Gamon, J., Fredeen, A., Merino, J., Field, C., 1994. Reflectance indices associated with physiological changes in nitrogen-and water-limited sunflower leaves. Remote Sens. Environ. 48, 135–146.
Poorter, H., Niinemets, Ü., Poorter, L., Wright, I.J., Villar, R., 2009. Causes and consequences of variation in leaf mass per area (LMA): a meta-analysis. New Phytol. 182, 565–588.
Pu, R., Gong, P., Biging, G.S., Larrieu, M.R., 2003. Extraction of red edge optical parameters from hyperion data for estimation of forest leaf area index. Ieee Trans. Geosci. Remote. Sens. 41 (4), 916–921.
Schneider, C.A., Rasband, W.S., Eliceiri, K.W., 2012. NIH Image to ImageJ: 25 years of image analysis. Nat. Methods 9, 671–675.
Serrano, L., Ustin, S.L., Roberts, D.A., Gamon, J.A., Penuelas, J., 2000. Deriving water content of chaparral vegetation from AVIRIS data. Remote Sens. Environ. 74, 570–581.
Tan, K., Cheng, X., 2016. Surface reflectance retrieval from the intensity data of a terrestrial laser scanner. JOSA A 33, 771–778.
Terashima, I., Hanba, Y.T., Tazoe, Y., Vyas, P., Yano, S., 2005. Irradiance and phenotype: comparative eco-development of sun and shade leaves in relation to photosynthetic CO2 diffusion. J. Exp. Bot. 57, 343–354.
Trumbore, S., Brando, P., Hartmann, H., 2015. Forest health and global change. Science 349, 814–818.
Valentinuz, O.R., Tollenaar, M., 2004. Vertical profile of leaf senescence during the grain-filling period in older and newer maize hybrids. Crop Sci. 44, 827–834.
Wang, Q., Li, P., 2013. Canopy vertical heterogeneity plays a critical role in reflectance simulation. Agric. For. Meteorol. 169, 111–121.
Yao, R.T., Scarpa, R., Turner, J.A., Barnard, T.D., Rose, J.M., Palma, J.H.N., Harrison, D.R., 2014. Valuing biodiversity enhancement in New Zealand's planted forests: socioeconomic and spatial determinants of willingness-to-pay. Ecol. Econ. 98, 90–101.
Yilmaz, M.T., Hunt Jr, E.R., Jackson, T.J., 2008. Remote sensing of vegetation water content from equivalent water thickness using satellite imagery. Remote Sens. Environ. 112, 2514–2522.
Zarco-Tejada, P.J., Rueda, C.A., Ustin, S.L., 2003. Water content estimation in vegetation with MODIS reflectance data and model inversion methods. Remote Sens. Environ. 85, 109–124.
Zhao, S., Wang, Q., Yao, Y., Du, S., Zhang, C., Li, J., Zhao, J., 2016. Estimating and validating wheat leaf water content with three MODIS spectral indexes: a case study in Ningxia Plain. China. Journal of Agricultural Science and Technology 18, 387–398.
Zheng, G., Ma, L., He, W., Eitel, J.U.H., Moskal, L.M., Zhang, Z., 2016. Assessing the contribution of woody materials to forest angular gap fraction and effective leaf area index using terrestrial laser scanning data. Ieee Trans. Geosci. Remote. Sens. 54, 1475–1487.
Zheng, G., Moskal, L.M., Kim, S.-H., 2013. Retrieval of effective leaf area index in heterogeneous forests with terrestrial laser scanning. IEEE Trans. Geosci. Remote Sens. 51, 777–786.
Zhu, X., Wang, T., Darvishzadeh, R., Skidmore, A.K., Niemann, K.O., 2015. 3D leaf water content mapping using terrestrial laser scanner backscatter intensity with radiometric correction. Isprs J. Photogramm. Remote. Sens. 110, 14–23.
Zhu, X., Wang, T., Skidmore, A.K., Darvishzadeh, R., Niemann, K.O., Liu, J., 2017. Canopy leaf water content estimated using terrestrial LiDAR. Agric. For. Meteorol. 232, 152–162.